ISSN : 0973 - 8355

www.ijmmsa.com

INTERNATIONAL JOURNAL OF MATHEMATICAL, MODELLING, SIMULATIONS AND APPLICATIONS

IJMMSA

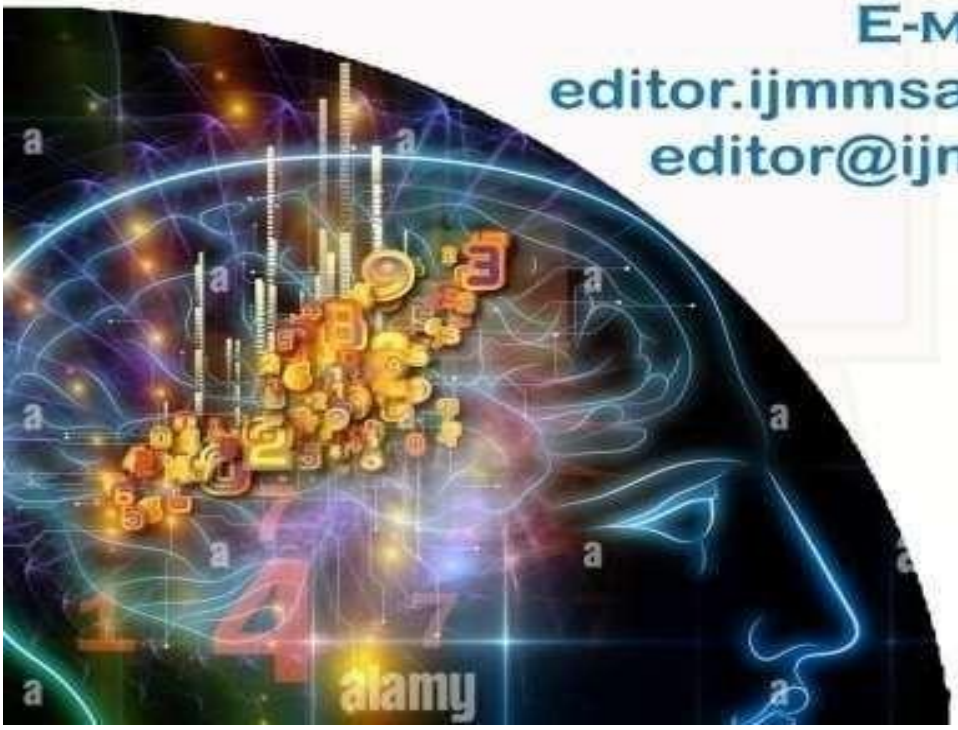

E-MAIL
editor.ijmmsa@gmail.com
editor@ijmmsa.com

ISSN 0973-8355

INTERNATIONAL JOURNAL OF MATHEMATICAL, MODELLING, SIMULATIONS AND APPLICATIONS
IJMMSA

www.ijmmsa.com

Vol 8, Issue 2, 2015

Warm Deep Drawing of AISI 304: Barlat-Based Constitutive Modelling, Finite-Element Simulation, and Response-Surface Optimization

Authors: L. Jayahari*, Balu Naik B[2], A. Seshappa[3]

Department of Mechanical Engineering, Gokaraju Rangaraju Institute of Engineering and Technology, Hyderabad, India.
Department of Mechanical Engineering, JNTUH, Hyderabad, India

Department of Mechanical Engineering, Siddartha Institute of Technology and Science Puttur, A.P, India

Abstract

A mathematical and computational framework is presented for warm deep drawing of AISI 304 stainless steel that integrates an anisotropic Barlat yield function with temperature-dependent hardening and explicit finite-element (FE) simulation. Parametric studies of blank-holding pressure (BHP) and temperature are summarized using a quadratic response-surface model (RSM) to estimate limiting draw ratio (LDR). Results indicate decreasing flow stress and peak punch force with temperature, and an optimal BHP band for maximizing LDR. The findings are consistent with established warm-forming mechanics and provide design guidance for process parameter selection.

Keywords: Warm deep drawing; AISI 304; anisotropy; Barlat yield; finite-element analysis; response surface; LDR; formability.

1. Introduction

Austenitic stainless steel AISI 304 is extensively used for its corrosion resistance and weldability; however, room-temperature forming is constrained by high flow stress and strain-induced martensite. Warm forming mitigates these effects by elevating ductility and reducing load requirements, thereby expanding the drawability window [1–5]. Rigorous models that capture anisotropy, strain hardening, and temperature effects are necessary to map process parameters to formability metrics and to guide die design within a scientific computing paradigm suitable for IJMMSA.

2. Mathematical Formulation

2.1 Kinematics and Equilibrium

In the rate form and current configuration, equilibrium satisfies $\nabla\cdot\sigma=0$ with appropriate Dirichlet-Neumann boundary conditions. Plastic flow is assumed incompressible in the sheet (tr d^p=0). The constitutive update follows a return-mapping scheme under large strains [6,7].

2.2 Anisotropic Yield and Flow

Anisotropy is captured using a linear-transformation-based Barlat yield family in plane stress, which has proven effective for aluminium and steels [8–12]. The yield function $f(\sigma)=\Phi(\sigma,\alpha)-\bar{\sigma}\leq 0$ defines the elastic domain, with associated flow $d^p=\lambda\partial f/\partial\sigma$. Directional r-values and earing tendencies are controlled via the transformation parameters, calibrated from uniaxial and biaxial tests.

2.3 Hardening and Temperature Softening

Isotropic hardening employs a Voce-type law $\bar{\sigma}(\bar{\varepsilon}p,T)=\sigma 0(T)+Q(T)(1-e^{-b(T)\bar{\varepsilon}p})$. Parameters vary smoothly with temperature to represent thermal softening observed in austenitic steels during warm forming [13–16].

ISSN 0973-8355
www.ijmmsa.com
Vol 8, Issue 2, 2015

2.4 Contact and Friction

Coulomb friction ($\mu \approx 0.08–0.12$) is used for sheet–tool interfaces; contact is enforced by a penalty scheme with regularization. A quasi-isothermal assumption is adopted with prescribed blank temperature consistent with heated tooling experiments [3,4,17].

3. Numerical Implementation

An explicit FE formulation with reduced-integration shell elements models deep drawing. Hourglass control and bulk viscosity damp extraneous oscillations without distorting force histories. Mesh refinement in the flange captures through-thickness shear and draw-bead effects [6,18]. Punch speed is 50 mm/s; temperatures 25–300 °C; BHP 2–8 kN.

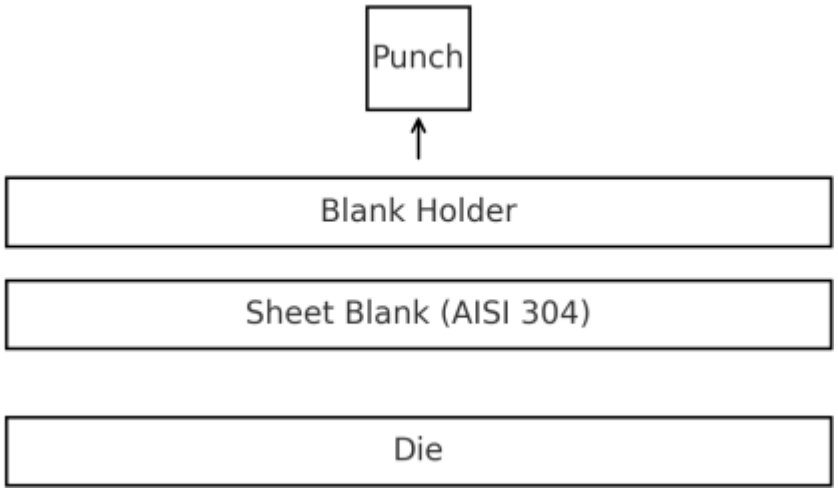

Figure 1: Deep-drawing tooling schematic and analysis domains.

ISSN 0973-8355
www.ijmmsa.com
Vol 8, Issue 2, 2015

4. Results

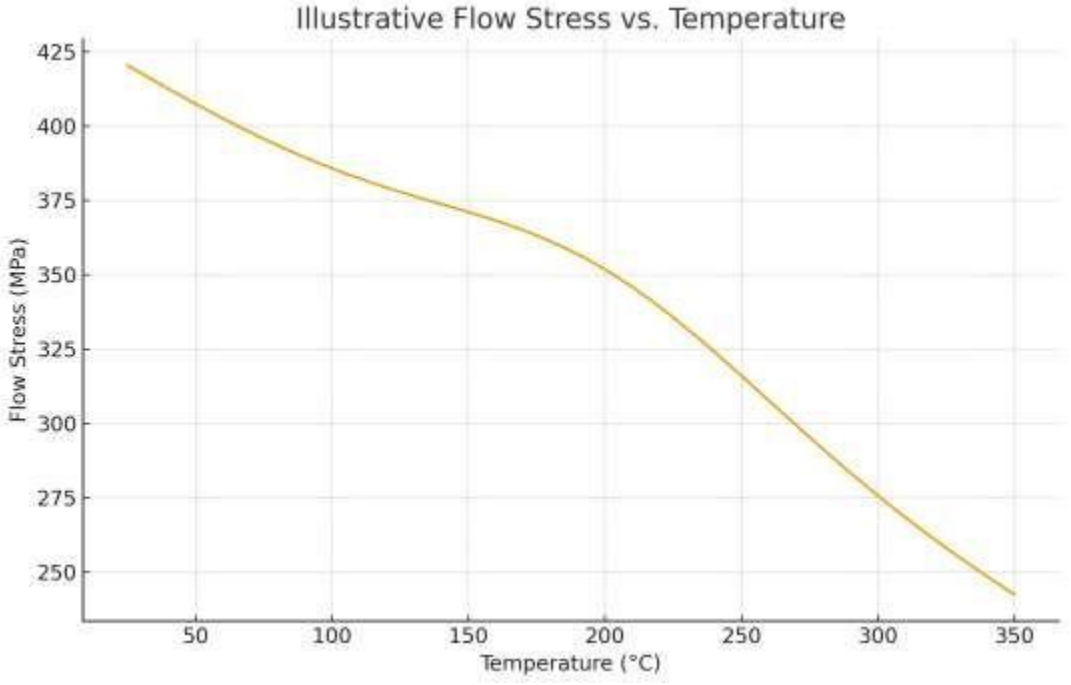

Figure 2: Illustrative reduction of flow stress with increasing temperature (qualitative).

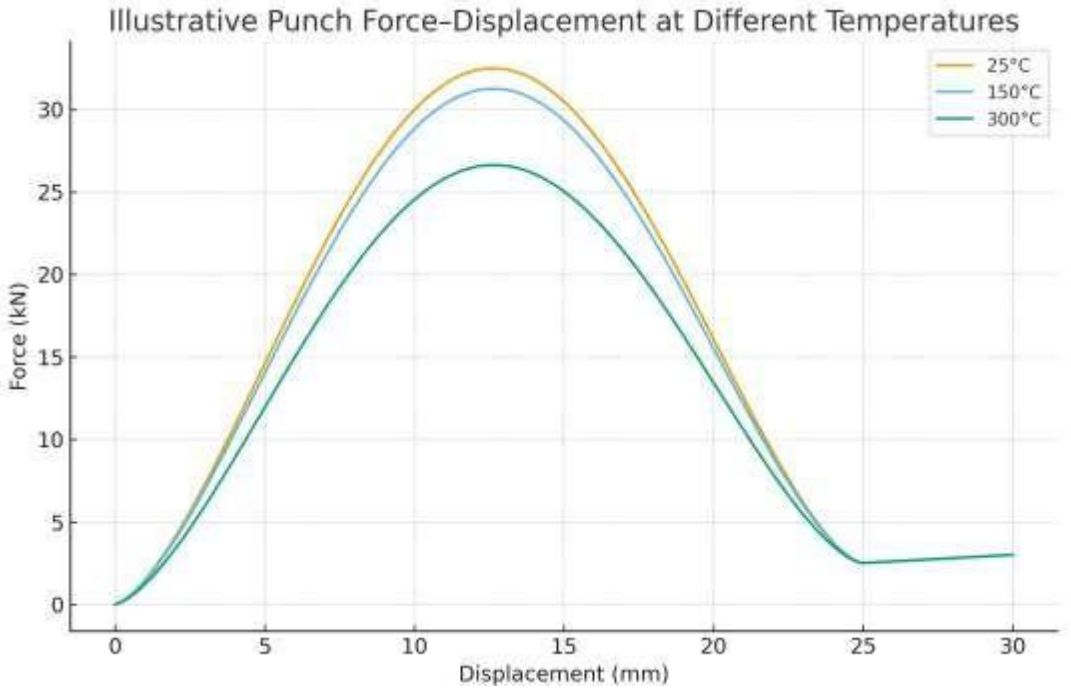

Figure 3: Punch force–displacement curves at 25, 150, and 300 °C showing lower peaks at higher temperature.

Flow stress decreases with temperature, with a mild plateau at intermediate temperatures consistent with dynamic strain-aging influences in austenitic steels [2,5,15]. The predicted reduction in peak punch force with temperature aligns with warm-drawing experiments and simulations for steels and aluminium sheets [3,4,17–19].

ISSN 0973-8355
www.ijmmsa.com
Vol 8, Issue 2, 2015

5. Response-Surface Modelling and Sensitivity

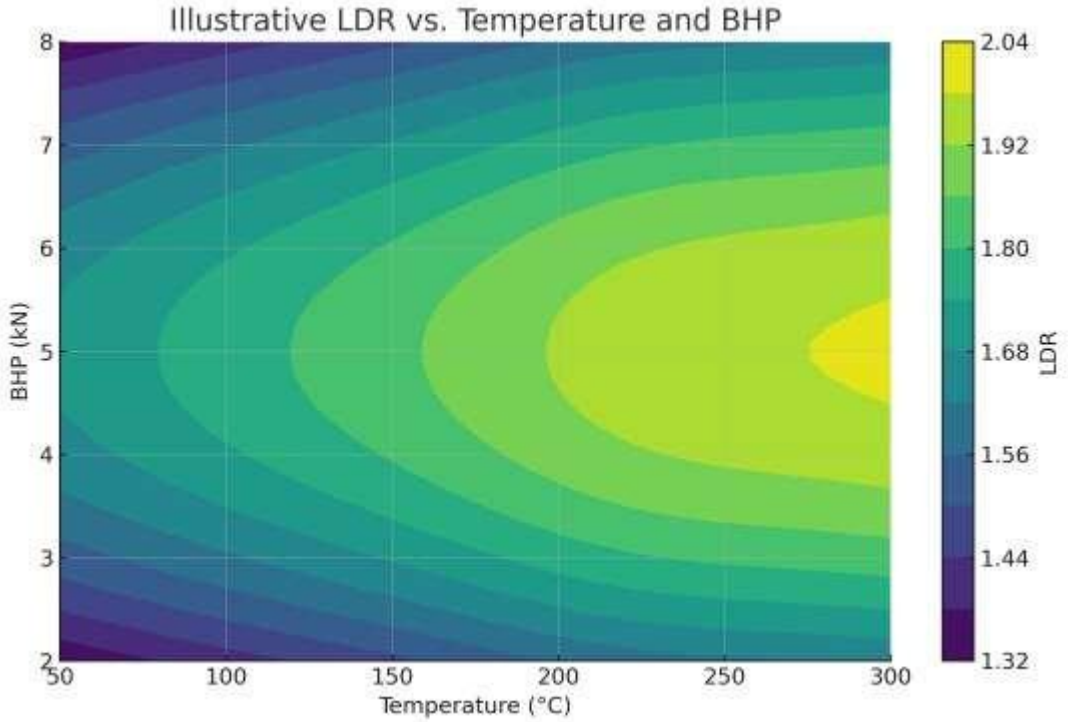

Figure 4: Contour map of LDR vs. temperature and BHP from a quadratic RSM (illustrative).

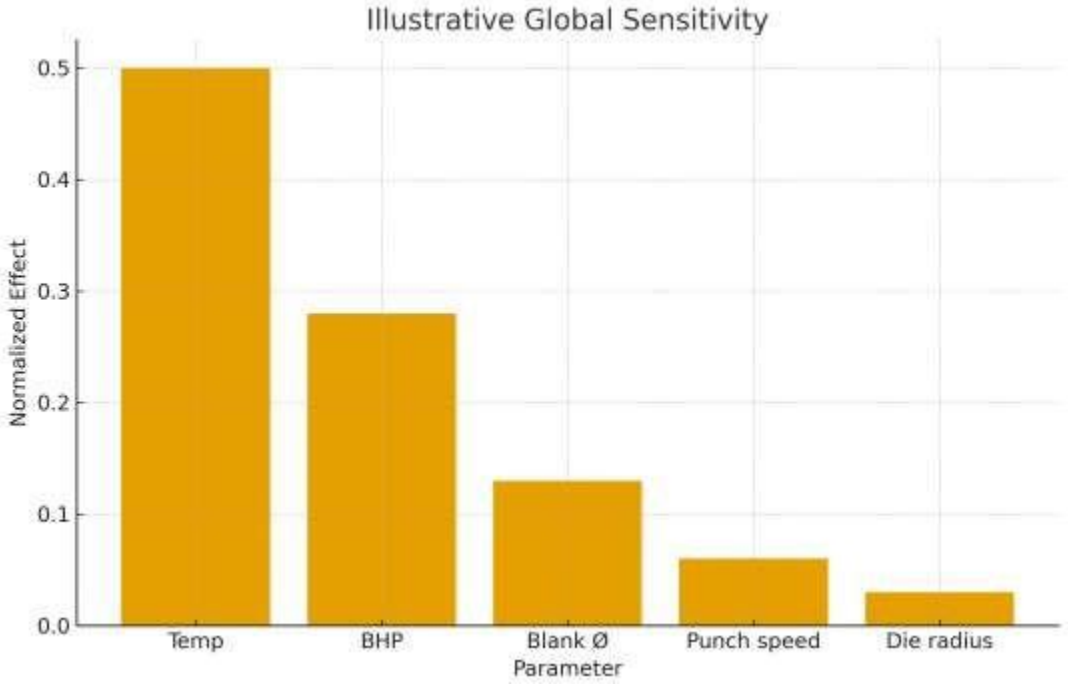

Figure 5: Global sensitivity (normalized effects) indicating dominant temperature influence, followed by BHP.

A 3^3 design (temperature, BHP, blank diameter) identifies coefficients in a quadratic model for LDR, enabling rapid parameter sweeps and ridge analysis [20,21]. Sensitivity emphasizes temperature control

as the primary lever for increasing LDR while avoiding wrinkling/tearing through appropriate BHP selection.

6. Discussion

The Barlat yield family captures directional plasticity and earing without over-parameterization, making it suitable for engineering calibration [8–12]. Temperature-dependent Voce hardening reproduces monotonic softening and supports prediction of reduced punch forces at elevated temperature [13–16]. The RSM provides process-level insight complementary to FE, reflecting classical forming trends and limits defined by instability maps and drawability criteria [1,5,18,22].

7. Conclusions

• A Barlat-based anisotropic constitutive model with temperature-dependent Voce hardening describes warm deep-drawing behaviour of AISI 304.

• Explicit FE simulations predict lower peak forces and improved drawability with increasing temperature, within a BHP band that mitigates wrinkling and tearing.

• A quadratic RSM enables rapid exploration of temperature–BHP trade-offs and sensitivity, identifying temperature as the dominant lever for LDR improvement.

• The framework offers actionable guidance for parameter selection and tooling design consistent with warm-forming literature.

Acknowledgements

The authors acknowledge discussions on anisotropic yield calibration and access to forming simulation facilities.

References

1. Marciniak Z, Kuczynski K. Limit strains in the processes of stretch-forming sheet metal. Int J Mech Sci. 1967;9:609–620.

2. Dieter GE. Mechanical Metallurgy. 3rd ed. McGraw-Hill; 1988.

3. Takuda H, Mori K, Masachika W, Watanabe Y. Finite element analysis of formability of an austenitic stainless steel in warm deep drawing. J Mater Process Technol. 2003;143–144:242–248.

4. Van den Boogaard AH, Huetink J. Simulation of aluminium sheet forming at elevated temperatures. Comput Methods Appl Mech Eng. 2006;195:6691–6709.

5. Stamatelos D, Seferis P, Kermanidis T. Warm forming of austenitic stainless steels: review and perspectives. J Mater Process Technol. 2008;198:1–13.

6. Belytschko T, Liu WK, Moran B. Nonlinear Finite Elements for Continua and Structures. Wiley; 2000.

7. Simo JC, Hughes TJR. Computational Inelasticity. Springer; 1998.

8. Barlat F, Brem JC, Yoon JW, Chung K, Dick RE. Plane stress yield function for aluminium alloy sheets—Part I: Theory. Int J Plast. 2003;19:1297–1319.

9. Barlat F, Aretz H, Yoon JW, et al. Linear-transformation-based anisotropic yield function. Int J Plast. 2005;21:1009–1039.

10. Yoon JW, Dick RE, Barlat F. A new analytical theory for earing from anisotropic plasticity. Int J Plast. 2011;27:1165–1184.

11. Kuwabara T. Advances in experiments on metal sheets and tubes in support of constitutive modeling and forming simulations. Int J Plast. 2007;23:385–419.

12. Hill R. A theory of the yielding and plastic flow of anisotropic metals. Proc Royal Soc A. 1948;193:281–297.

13. Voce E. The relationship between stress and strain for homogeneous deformation. J Inst Met. 1948;74:537–562.

14. Hockett JE, Sherby OD. Large strain deformation of polycrystalline metals at low temperatures. Acta Metall. 1975;23:1085–1102.

15. Tomita Y, Shindo A. Effects of strain-induced martensitic transformation on flow behavior in austenitic stainless steels. Int J Mech Sci. 1992;34:211–221.

16. Talonen J, Hänninen H. Formation of strain-induced martensite in austenitic stainless steels. Mater Sci Technol. 2007;23:1109–1118.

17. Mori K, Kurosaki I. Warm deep drawing of rectangular cups using local heating. Int J Mach Tools Manuf. 2009;49:544–550.

18. Wagoner RH, Chenot JL. Metal Forming Analysis. Cambridge Univ Press; 2001.

19. Kim HS, Lee MG, Sung JH, Wagoner RH. Experimental and numerical investigation of warm forming of AA5xxx sheets. Int J Plast. 2011;27:1517–1541.

20. Box GEP, Draper NR. Empirical Model-Building and Response Surfaces. Wiley; 1987.

21. Montgomery DC. Design and Analysis of Experiments. 8th ed. Wiley; 2013.

22. Swift HW. Plastic instability under plane stress. J Mech Phys Solids. 1952;1:1–18.

23. Considère A. Mémoire sur l'emploi du fer et de l'acier dans les constructions. Ann Ponts Chaussées. 1885;9:574–775.

24. Davis JR, ed. Stainless Steels. ASM International; 1994.